applied sciences

MDPI

Article

Mechanical Properties of Sheet Pile Cofferdam during Adjacent Open Cut Tunnel Construction near Lake Bottom

Chuang Kai and Jinming Xu *

Department of Civil Engineering, Shanghai University, Shanghai 200444, China
* Correspondence: xjming211@163.com

Abstract: In water-related projects, the application of steel sheet pile cofferdams is becoming more and more widespread, and the influence of tunnel construction on the mechanical properties of adjacent cofferdams is important. In this study, the object of research was the mechanical properties of large-span steel sheet pile cofferdams. The open-cut tunnel project was located in Suzhou Yinshan Lake, China. According to the actual construction steps of the tunnel foundation pit, assuming that the soil was a small strain hardening soil model, combined with on-site monitoring data, a three-dimensional elastoplastic finite difference model was established. The results show that during tunnel construction, the maximum settlement of the cofferdam appeared at 0.27~0.53 m on the side of the foundation pit; the maximum horizontal displacement of the steel sheet pile occurred at the pile bottom of foundation pit side, and the seepage gradually increased during construction, eventually resulting in water gushing at the bottom of the foundation pit. After the completion of tunnel construction, the settlement value of the cofferdam presented a pattern that first increased and then decreased from the side of the foundation pit to the side of the adjacent lakeside; the steel cofferdam tilted toward the side of the foundation pit, with a maximum inclination angle of 3.37°. It should be pointed out that as the construction progressed, the axial force of the tie rods in the steel cofferdam changed from a U-shaped distribution to a V-shaped distribution. This study could provide a reference for the impact of tunnel foundation pit construction on adjacent steel cofferdam and could also provide a reference for the safety research of open-cut tunnel construction.

Keywords: cut-and-cover tunnel; double sheet pile cofferdam; mechanical properties; finite difference method

Citation: Kai, C.; Xu, J. Mechanical Properties of Sheet Pile Cofferdam during Adjacent Open Cut Tunnel Construction near Lake Bottom. *Appl. Sci.* **2023**, *13*, 6191. https://doi.org/10.3390/app13106191

Academic Editor: Cheng-Yu Ku

Received: 12 April 2023
Revised: 11 May 2023
Accepted: 17 May 2023
Published: 18 May 2023

1. Introduction

Due to its advantages, such as good water tightness, space-saving, and easy construction, steel sheet pile cofferdams are increasingly widely used in water-related projects in China and abroad [1,2]. However, due to the complexity of foundation pit construction and hydrogeological engineering conditions, steel sheet pile cofferdams can easily become uncertain factors in engineering safety.

This study explored the double-row steel sheet pile cofferdam tunnel project on the bank of Suzhou Yinshan Lake. Due to the close distance between the cofferdam and the tunnel, tunnel construction is prone to disturb the cofferdam. Therefore, the problem of the influence of tunnel construction on the mechanical properties of double-row steel sheet pile cofferdam needed to be studied. Double-row steel sheet pile cofferdams are usually used for water-related projects or deep foundation pit engineering [1]. Byfield and Crawford [2] and Bourn et al. [3] conducted experiments and research on the deformation characteristics of steel sheet piles, providing some suggestions for the stress analysis of steel sheet piles and a study of the pile–soil interaction mechanism. Osthoff and Jurgen [4] used the Euler-Lagrange coupling method for numerical analysis to study the stress and deformation characteristics of steel sheet piles during the driving process. Lefas and Georgiannou [5] established a two-dimensional simplified model to analyze the stress and deformation characteristics of steel sheet piles during construction. Gui and Han [6] studied the failure of the cofferdam and found that the main reason for the failure of the double-wall cofferdam was the dislocation of the weld. Shao et al. [7], based on finite element calculations, summarized the relationship between the design parameters and the structural response of steel sheet pile cofferdam through optimization algorithms and design experiments. Yan et al. [8] compared and analyzed indoor and centrifugal machine tests to reveal the factors affecting the lateral bearing capacity of the double-row steel sheet pile cofferdam. The Finite element analysis model was used to analyze the seepage path and seepage flow rate of water in the steel sheet pile cofferdam [9,10]. Fukumoto et al. [11] studied the basic problems of steel sheet pile seepage failure through a two-dimensional fluid-solid coupling model. The fully coupled three-dimensional nonlinear finite element analysis method was adopted. The dynamic response of a single pile in liquefiable sand under a bidirectional load is studied [12]. Xu et al. proposed a numerical solution to evaluate the cofferdam collapse block and landslide thrust patterns based on a power-law nonlinear damage criterion and limit analysis. Parametric studies were used to optimize the cofferdam design and improve the stability analysis [13]. Steel sheet piles were used as pile foundations with a large surface area and high strength to improve the bearing capacity. Model tests were conducted using the OFDR technique, and the results showed its strain distribution characteristics [14]. The effect of the surface roughness of steel sheet piles on the lateral bearing behavior of piles embedded in the sand was investigated. It was found that the surface roughness of the piles significantly affected their lateral bearing capacity [15]. Doubrovsky et al. studied the parameters of sheet pile walls made from U-shaped piles interacting with the soil through full-scale physical models and laboratory simulations, and analyzed the effect of soil friction and resistance in the interlocking body [16].

There were also some research results on the numerical simulation of tunnel construction. In the numerical study of a deep tunnel, Schreter et al. [17] carried out numerical model calculations based on advanced material models, which provided important insights into the potential failure mechanism of deep tunnel structures. Liao et al. [18] systematically studied the brittle failure of buried pipelines caused by ground subsidence and tunnel excavation through a centrifuge tests and numerical simulations. Scholars studied the influence of tunnel construction on the surrounding environment through numerical models [19–21]. Li et al. [22] carried out model test and numerical simulation on the construction progress of the Daling tunnel. By monitoring the deformation and stress changes of the surrounding rock in real time, they studied the mechanical response law and revealed the mechanical characteristics of large-span and small-span tunnels during construction. Glenda Abate et al. [23] studied the dynamic interaction between the tunnel, soil and buildings on the ground through fully coupled FEM modeling and also studied the influence of the tunnel on soil and building response.

The current research mainly focuses on the influence of construction and structural parameters of cofferdams on their own deformation, while relatively little research has been conducted on the influence of tunnel foundation pit construction or on the deformation characteristics of the double-row steel sheet pile cofferdam. Wu et al. [24] used a finite difference model to evaluate the deformation of double-row steel sheet piles in deep foundation pit construction and summarized the rules that influenced the inclination angle, pile diameter, penetration depth, and row spacing of deformation. Finite element software was used to study the mutual influence between deep foundation pits and cofferdams and found that the excavation of foundation pits mainly caused the horizontal deformation on the lower part of the cofferdam pile foundation to increase [25,26]. Fall et al. [27] studied the influence of tunnel foundation pit construction on the mechanical properties of the adjacent steel sheet pile wall through the finite element mode and found that the unpredictable displacement and bending moment occurred at the top of the wall during backfilling. The short-term water level prediction model of the support vector machine was established. This model could accurately predict the short-term water level, ensuring the construction of the steel sheet pile cofferdam [28]. Zhao et al. performed a sensitivity analysis to investigate the mechanism of the soil–structure interaction system by numerically simulating the behavior of the anchored sheet pile wall structure during excavation and backfill construction [29].

The geological and environmental conditions of hydro-engineering projects could lead to major construction accidents in cofferdams, and the influence of the tunnel foundation pit construction on adjacent cofferdams is still an urgent subject to be studied. In this study, the large-span steel sheet pile cofferdam in the Suzhou Yinshan Lake Tunnel Project was taken as the research object. The finite difference software FLAC3D 6.0 was used to establish a three-dimensional numerical analysis model of open-cut tunnel construction and adjacent steel sheet pile cofferdams. By comparing the numerical simulation results with the field monitoring results, the influence of tunnel construction on the mechanical properties of steel sheet pile cofferdam construction could be studied.

2. Overview of the Project and Layout of Measurement Points

The Suzhou Yinshan Lake Tunnel Project was the second phase of the international fast logistics channel project. The main line of the NHLDY-SG02 section of the east Extension Project of Nanhu Road Expressway passed through Yinshan Lake West Road, Central River and Yinshan Lake in the form of a tunnel. Among them, the open section was 200 m, and the tunnel was 1.9 km (1.1 km through the Yinshan Lake section). Crossing the middle section of Yinshan Lake, the cofferdam was closed, and then backfilling was carried out to design the elevation for foundation pit construction. The project plan is shown in Figure 1.

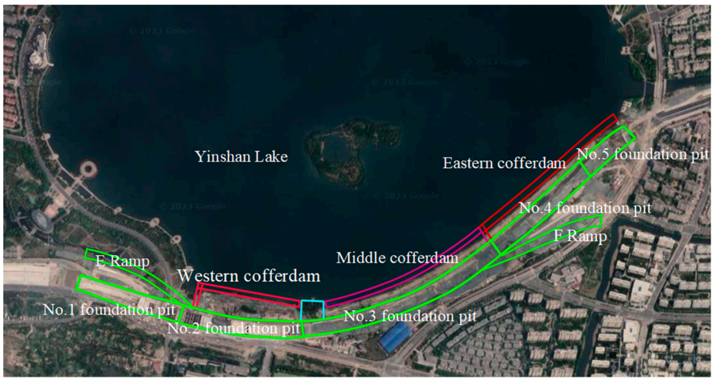

Figure 1. Project plan.

The bottom elevation of Yinshan Lake was mostly between −1.00 m and −8.50 m, and the total length of the cofferdam in the lake was 1.61 km. The double-row steel sheet pile cofferdam was used as a temporary water-retaining structure. During construction, backfill soil was compacted from the shore to the lake, steel sheet piles were driven to the top of the slope, and double-row steel sheet piles were connected into a whole by the tie bars. After the completion of the cofferdam construction, the open-cut tunnel construction in the lake was carried out. The tunnel was mainly located on the south side of the cofferdam, and open-cut construction was adopted. At the same time, dewatering was carried out in the foundation pit. Figure 2 depicts the schematic diagram of the cross-section of the cofferdam. Measurement points are set every 50 m along the axis of the cofferdam to observe the displacement and settlement of the cofferdam (see Figure 3).

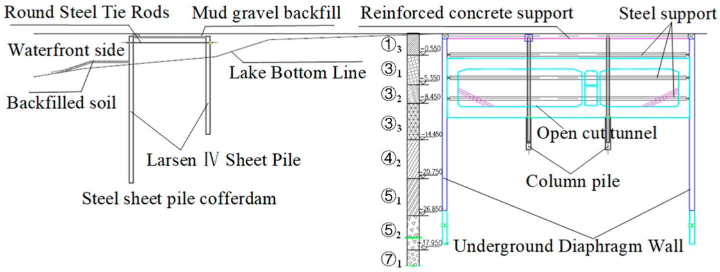

Figure 2. Cross-section of cofferdam.

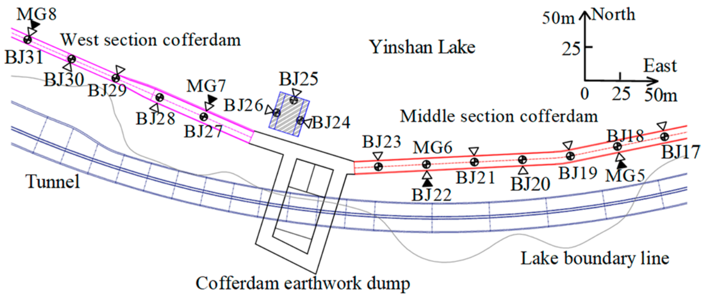

Figure 3. Locations of measurement points for cofferdam deformation and tie rod axial forces.

3. Establishment of Numerical Analysis Models

3.1. Geometric Models and Boundary Conditions

The tunnel foundation pit construction adopted the open-cut method. Figure 4a shows the overall appearance of the numerical analysis model of the tunnel and steel sheet pile cofferdam. In this model, X represented the horizontal direction, with the east as the positive direction of the X-axis, Y represented the direction of the tunnel extension, with the north as the positive direction of the Y-axis, Z represented the depth direction of the foundation pit, with the upward direction as the positive direction of the Z-axis, and the lake's bottom was located on the left side of the foundation pit. To eliminate the influence of boundary effects, the left range of the foundation pit was taken as five times the construction depth of the tunnel foundation pit, the right and bottom ranges were taken as four times the construction depth of the tunnel foundation pit, and the length direction of the tunnel was taken as 30 m. The material parameters of the sheet pile cofferdam and enclosure structure are shown in Table 1.

Table 1. Material parameters of retaining structure and sheet pile cofferdam.

Type of Material	Density (g/cm^3)	Elastic Modulus (MPa)	Poisson's Ratio (-)
Larsen VI Sheet Pile	8.01	206,000	0.31
Round Steel Tie Rod	7.95	200,000	0.20
Underground Diaphragm Wall	2.45	31,500	0.20
Concrete support	2.38	30,000	0.20
Steel support	7.85	200,000	0.20
Column pile	2.50	30,000	0.20
Backfilled soil	1.85	20	0.20

The depth of the foundation pit was 13.8 m, and the width was 40 m. In the foundation pit's supporting structure, the top layer was concrete support with a size of 0.8 m $\times$ 0.8 m, and the lower three layers were steel supports with a diameter of 0.69 m and a thickness of 0.0016 m. The diameter of the drill-pouring pile was 0.85 m, and the length was 30 m. The underground continuous wall was composed of C35 concrete, and the thickness of the underground continuous wall was 0.8 m. The cofferdam was 18 m away from the foundation pit, which is the minimum distance from the foundation pit of the Yinshan Lake

Tunnel Project. The cofferdam structure adopted Larsen IV steel sheet piles, and the length of steel sheet piles on the adjacent lakeside was 23 m; the length of steel sheet piles on the pit side was 17 m, and the width of the cofferdam was 8 m. In the steel sheet pile cofferdam structure, there were 15 round steel tie rods with a diameter of 0.048 m and spacing of 2 m. The steel cofferdam and tunnel construction supporting structure are shown in Figure 4b.

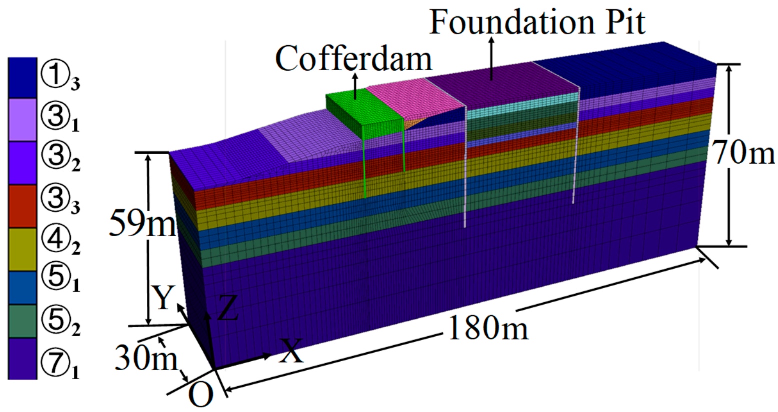

(**a**)

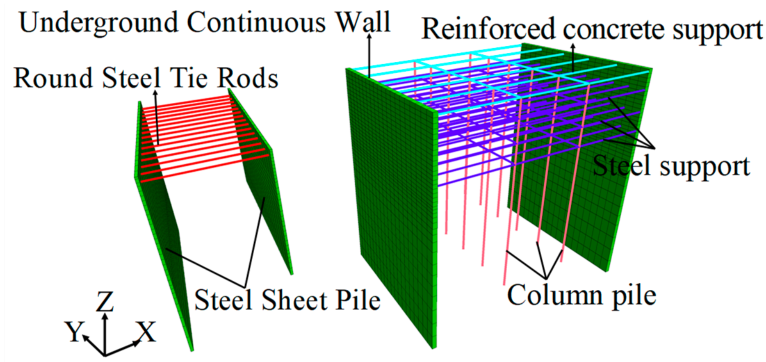

(**b**)

Figure 4. Geometry model of tunnel construction and sheet pile cofferdam. (**a**) Whole model. (**b**) Steel cofferdam and tunnel construction supporting structure.

The mesh model was modeled and meshed by the finite element software Abaqus and then converted into a mesh file in the Flac3d format, which was called the calculation file. The model was then divided into 94,437 nodes and 87,060 hexahedral meshes.

The boundary conditions in the numerical analysis model included the surface around the model, restricted normal displacement, and the bottom, which restricted the displacement in X, Y, and Z directions. The groundwater level was considered according to the design water level and was set at 1.5 m below ground level.

The water pressure above the lake bottom was applied in loading form. The lake's bottom surface adopts a fixed head boundary. When the groundwater was lowered below the construction surface in time during the foundation pit construction, it could be assumed that there waso water in the foundation pit during construction and that the seepage of groundwater in the soil followed Darcy's law.

3.2. Determination of Soil Parameters

According to the survey report, the bottom soil layers from top to bottom were①$_3$—plain fill,③$_1$—clay,③$_2$—silty clay,③$_3$—silt,④$_2$—silty sand mixed with silt,⑤$_1$—silty clay mixed with silty sand,⑤$_2$—silty sand mixed with silty clay,⑦$_1$—silty clay (distribution location as shown previously in Figure 4a).

The physical and mechanical properties parameters of each soil layer are shown in Table 2. In the table, the natural unit weight, compression modulus, cohesion force, internal friction angle, void ratio and permeability coefficient were determined based on the survey report.

Table 2. Physical and mechanical parameters of soil layers.

Soil Layer	H (m)	γ (kN/m^3)	e (-)	K (MPa)	E (MPa)	μ (-)	c (kPa)	φ (°)	k (cm/s)
①$_3$	0.55	18.5	0.860	6.88	23.85	0.33	12.0	10.0	/
③$_1$	5.35	19.5	0.750	6.22	35.20	0.28	41.2	14.4	3.05×10^{-7}
③$_2$	8.45	19.0	0.854	5.36	15.30	0.29	27.3	18.0	4.50×10^{-6}
③$_3$	14.45	18.7	0.756	12.61	24.10	0.23	7.1	23.5	6.09×10^{-4}
④$_2$	20.75	19.1	0.742	13.58	29.50	0.22	4.3	28.5	3.53×10^{-4}
⑤$_1$	26.85	19.0	0.869	5.09	13.90	0.35	7.7	17.7	2.12×10^{-5}
⑤$_2$	37.95	19.0	0.767	7.33	16.5p	0.35	4.9	23.6	5.45×10^{-5}
⑦$_1$	70.00	18.6	0.822	5.92	15.40	0.33	18.0	18.0	5.00×10^{-6}

Notes: H is embedment depth of foundation; γ is natural unit weight; e is void ratio; K is compressive modulus; E is elastic modulus; μ is Poisson's ratio; c is cohesion force; φ is internal friction angle; k is permeability coefficient.

3.3. Selection of Constitutive Model

According to the research of Gu Xiaoqiang et al. [30], the small strain hardening model (HSS model) could reasonably consider the nonlinearity, stress correlation and other characteristics of the modulus of elasticity in the elastic (small strain) stage of the soil; at the same time, the unloading deformation path corresponding to the unloading elastic modulus could no longer be applied after unloading. Therefore, this study adopted the HSS model as the constitutive model of soil.

The HSS model contained 13 parameters, including four strength-related parameters (effective cohesion of soil c', effective internal friction angle φ' of soil, dilation angle of soil ψ, and failure ratio determined by triaxial drained shear test R_f), seven stiffness-related parameters (reference stress p^{ref}, tangent modulus determined by standard consolidation test E_{oed}^{ref}, reference secant modulus determined by triaxial consolidation drained shear test E_{50}^{ref}, loading and unloading modulus determined by triaxial consolidation drained loading and unloading test E_{ur}^{ref}, loading and unloading Poisson's ratio v_{ur}, coefficient of static lateral pressure K_0, modulus stress level index m), and two small strain characteristic parameters (actual initial shear modulus G_0 and shear strain value $\gamma_{0.7}$ corresponding to shear modulus attenuation to 70% of the initial shear modulus). The parameters of the HSS model used were determined based on the survey report and triaxial consolidation undrained test (see Table 3).

Table 3. Parameters in constitutive model.

Soil Layer	c' (kPa)	φ' (°)	ψ (°)	E_{oed}^{ref} (MPa)	E_{50}^{ref} (MPa)	E_{ur}^{ref} (MPa)	G_0 (MPa)	K_0
①$_3$	4.0	25.0	5	6.19	8.26	48.16	192.64	0.5
②$_1$	0	30.0	0	5.60	7.46	43.54	174.16	0.5
③$_2$	17.0	23.1	0	4.82	6.43	37.52	150.08	0.5
③$_2$	3.0	12.6	0	12.50	15.50	89.00	355.00	0.5
④$_2$	6.0	33.0	10	12.22	16.30	95.06	380.24	0.3
⑤$_1$	11.9	23.7	5	4.58	6.11	35.63	142.52	0.5
⑤$_2$	3.2	26.8	5	6.60	8.80	51.31	205.24	0.3
⑦$_1$	9.8	20.4	0	26.15	35.50	207.20	828.80	0.6

Note: R_f take 0.95; p^{ref} take 100 kPa; v_{ur} take 0.2; m take 0.8; $\gamma_{0.7}$ take 2.0×10^{-4}.

3.4. Modelling of Steel Sheet Piles

The geometric section of Larsen IV steel sheet piles is relatively complex (see Figure 5 for the section size).

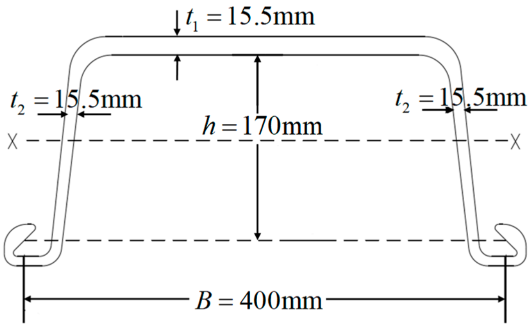

Figure 5. Section sizes of steel sheet piles.

For the convenience of modeling, the geometric section of the steel sheet pile was equivalent to a rectangular section with equal section moment according to the 'equivalent bending section modulus method', and the width and height of the rectangular section as B and h_0, respectively. Among them, B = 400 mm, and the calculation formula for h_0 can be shown as:

$$\left(\frac{B \times t_1^3}{12} + t_1 B h^2\right) + \left(\frac{t^2 \times h^3}{12} + \frac{t_2 h^3}{4}\right) \times 2 = \frac{B h_0^3}{12} \tag{1}$$

Calculated from Equation (1), h_0 = 190 mm. Due to the upper and lower interlocking of the steel sheet piles, the thickness of each steel sheet pile unit was twice the equivalent thickness of a single steel sheet pile (380 mm).

3.5. Validation of Model Correctness

Based on the comparison of the monitoring results of the deformation and internal force of steel cofferdam and tie rods with the numerical simulation results, the correctness of the established numerical analysis model could be verified.

For the deformation of the steel cofferdam, measurement points were set every 50 m along the axis of the cofferdam, and measurement points BJ17 to BJ23 and BJ27 to BJ31 (a total of 12 points) were selected. A comparison between the monitoring results settlement and numerical simulation results of steel cofferdam is shown in Figure 6a, and the comparison between the monitoring results and numerical simulation results of steel cofferdam horizontal displacement is shown in Figure 6b. For the internal force of the steel cofferdam tie rod (the tension is positive), three sets of measurement points, MG5, MG6 and MG7, were taken. The comparison between the monitoring results and the numerical simulation results is shown in Figure 6c.

From Figure 6a,b, it can be seen that after construction, the simulated values of the steel cofferdam settlement and horizontal displacement at each monitoring point were basically consistent with the monitoring value changes, indicating that the numerical analysis model was reliable. The simulated average settlement value at each monitoring point was 31.8% higher than the monitoring result, and the simulated average horizontal displacement value was 21.6% higher than the monitoring result. The possible reasons for this are: (1) the numerical model did not consider the effect of time on water seepage in the lake, resulting in a simulated value for the steel cofferdam settlement that was greater than the monitoring value; (2) during simulation, double-row steel sheet piles and tie rods were arranged in the steel cofferdam at the same time, while in the actual project, double-layer steel sheet piles were first constructed, followed by round steel tie rods, forming a complete steel cofferdam. The different construction sequences of round steel tie rods resulted in the simulated value of steel cofferdam displacement, which was greater than the monitoring value.

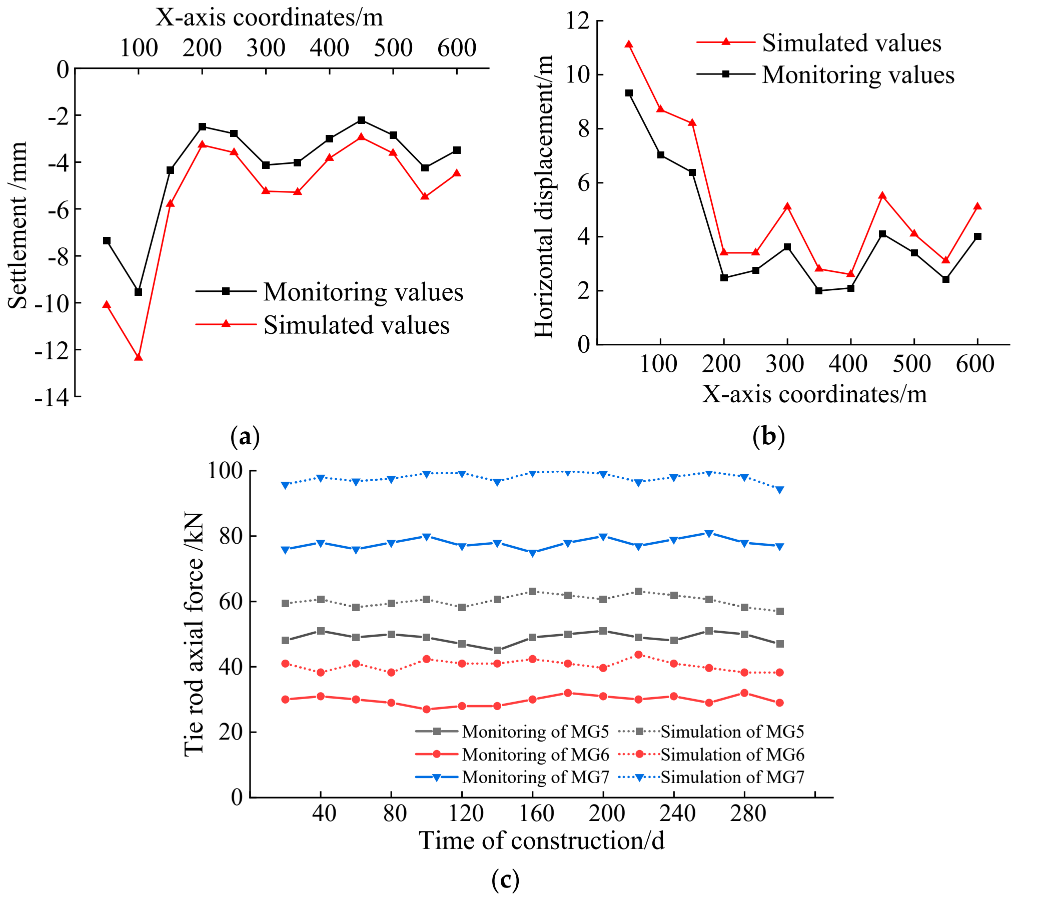

Figure 6. Monitored and simulated steel cofferdam horizontal and vertical deformations and tie rod axial forces. (**a**) Settlement of steel cofferdam. (**b**) Horizontal displacement of steel cofferdam. (**c**) Axial force of tie rods.

It can be seen from Figure 6c that the simulated internal force of the tie rod of the steel cofferdam was tension, and the variation law was basically consistent with the monitoring values. Since the steel cofferdam tie rod played the role of limiting the displacement of the double-layer steel sheet pile, the upper end of the double-layer steel sheet pile existed far away from the center of the steel cofferdam, and the internal force of the tie rod took on tension as a whole. The maximum internal force simulation value was in MG7, followed by MG5, and the minimum was in MG6. This is basically consistent with the pattern reflected by the monitoring value, which further verified the reliability of the numerical analysis model. The simulation results of the average internal force values of the three measurement points MG5, MG6, and MG7 were, respectively, greater than the monitoring values by 23.1%, 39.8%, and 25.6%. The reason why numerical simulations significantly predicted a force larger than the observed data was that the double-row steel sheet piles and ties in the steel cofferdam were arranged simultaneously in the simulation, while the actual double-row steel sheet piles and ties were not arranged simultaneously; the stress in the soil was released instantaneously in the simulation while the actual construction process was slow; the physical and mechanical properties of the materials used in the simulation were mostly the results of indoor tests, which could differ from the actual situation.

4. Analysis of the Mechanical Properties of Steel Sheet Pile Cofferdam Construction

4.1. Construction Conditions

Based on the calculation of the initial stress and initial pore water pressure field according to the original lake bottom slope line, a numerical analysis model of the steel sheet pile cofferdam construction was established according to the actual construction conditions. The construction conditions were as follows:

(1) Construction condition 0: Balancing the ground stress and construction cofferdam;

(2) Construction condition 1: Excavation and construction of the first concrete support (−0.45 m);

(3) Construction condition 2: Excavation and construction of the second steel support (−3.5 m)

(4) Construction condition 3: Excavation and construction of the third steel support (−7.25 m);

(5) Construction condition 4: Excavation and construction of the fourth steel support (−10.7 m)

(6) Construction condition 5: Excavation and construction of the tunnel (−13.8 m);

(7) Construction condition 6: Back-filling with soil cover.

Based on the numerical simulation results of the steel sheet pile cofferdam under different construction conditions, the mechanical properties of the steel sheet pile cofferdam during and after construction were analyzed, respectively.

4.2. Mechanical Characteristics of Steel Sheet Pile Cofferdam during Construction

(1) The settlement of steel cofferdam

To study the effect of the tunnel's construction on the deformation of adjacent steel sheet pile cofferdams, the simulated values of the settlement on the steel sheet pile cofferdam from the side of the adjacent lake to the side of the foundation pit were extracted from working conditions 1 to 6, and the relationship between the settlement of the cofferdam top and the horizontal distance was obtained (see Figure 7).

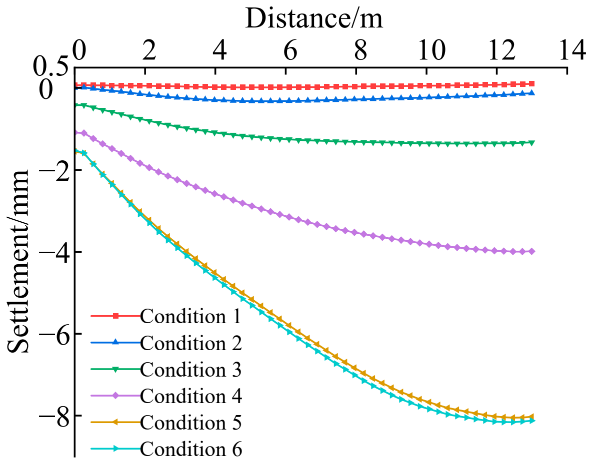

Figure 7. Settlements on cofferdam top at various horizontal distances.

It can be seen from Figure 7 that the maximum settlement of the cofferdam increased gradually with the construction. During the construction, the maximum settlement appeared on the side near the foundation pit, at a distance of 0.27~0.53 m; after the completion of construction condition 6, the maximum settlement was 8.16 mm.

(2) Horizontal displacement of steel cofferdam

The simulation results of the horizontal displacement of the steel sheet piles cofferdam at different positions and depths during tunnel construction are shown in Figure 8.

From Figure 8a, it can be seen that under the influence of multiple factors such as water pressure and soil pressure, the maximum horizontal displacement of the steel sheet pile cofferdam on the side adjacent to the lake always appeared at a depth of 11.27–12.67 m under different construction conditions. With the progress in construction, the maximum horizontal displacement gradually increased. After the completion of construction condition 6, the maximum horizontal displacement (0.12 mm) appeared at a depth of 11.73 m, indicating that the backfill of the soil and geotextile on the side adjacent to the lake could effectively restrain the horizontal displacement of the cofferdam on the side adjacent to the lake.

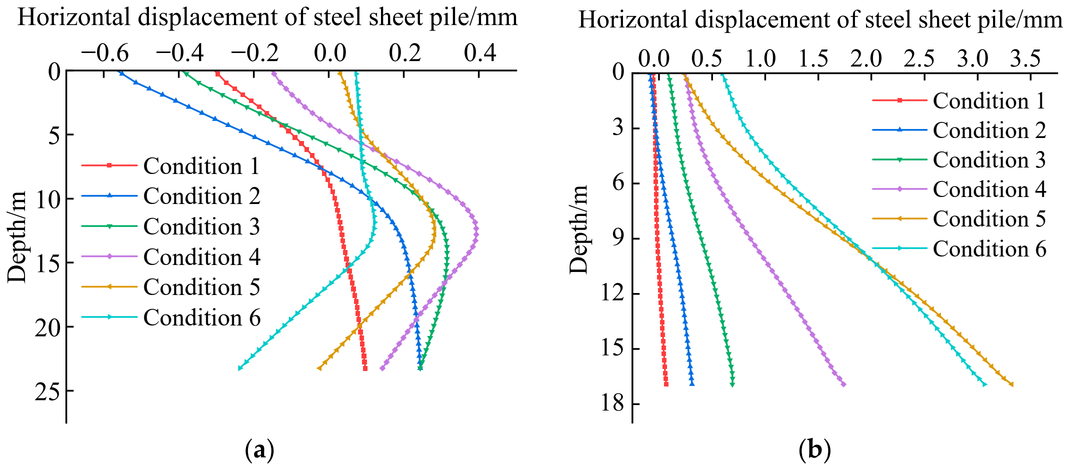

Figure 8. Relationship between depth and horizontal displacement of cofferdam. (**a**) Adjacent lakeside. (**b**) Foundation pit side.

From Figure 8b, it can be seen that the lateral steel sheet pile of the foundation pit was mainly affected by soil pressure, and the horizontal displacement of the steel sheet pile gradually increased with depth; the maximum horizontal displacement of the sheet pile under different construction conditions always appeared at the bottom of the steel sheet pile, and the average horizontal displacement of the lateral steel sheet pile of the foundation pit was greater than that of the adjacent lakeside; after the completion of construction condition 6, the maximum horizontal displacement (2.92 mm) appeared at the bottom of the steel sheet pile.

(3) Axial force on tie rod in steel cofferdam

Fifteen round steel tie rods were arranged within a 30 m tunnel length range. The eighth rod, located in the middle position, was selected, and the tie rod axial force under different construction conditions was extracted. The simulation results of the tie rod axial force at different positions on the side of the adjacent lake are shown in Figure 9.

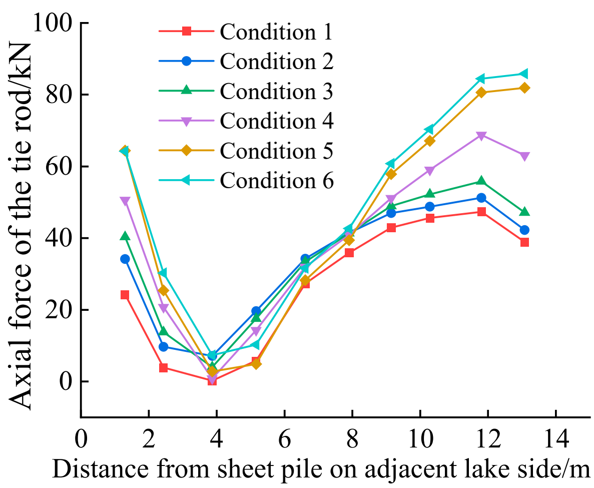

Figure 9. Monitored axial forces of tie rods adjacent to the lake at various distances.

From Figure 9, it can be seen that maximum tension appeared in the lateral tie rod of the adjacent lake; from the adjacent lakeside to the foundation pit side, the internal force of the tie rod gradually decreased, decreased to a minimum value at a distance 3.87 m from the lake, and then gradually increased to the maximum tension, showing a U-shaped distribution overall.

(4) Water seepage in the lake

The simulation results of the seepage path of lake water in the cofferdam under different construction conditions are shown in Figure 10. From Figure 10, it can be seen that water in the lake could flow around the steel sheet pile; as the construction progressed, the seepage gradually increased, and water could gush out at the bottom of the foundation pit.

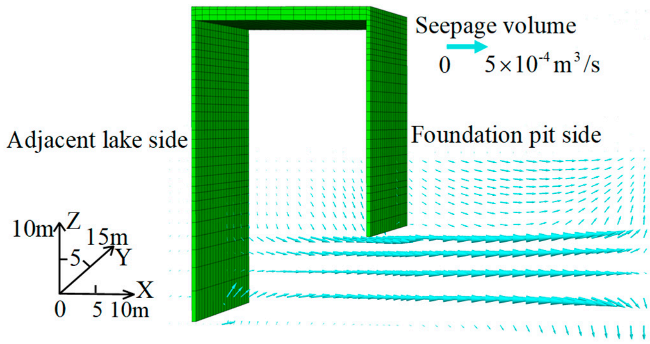

(**a**)

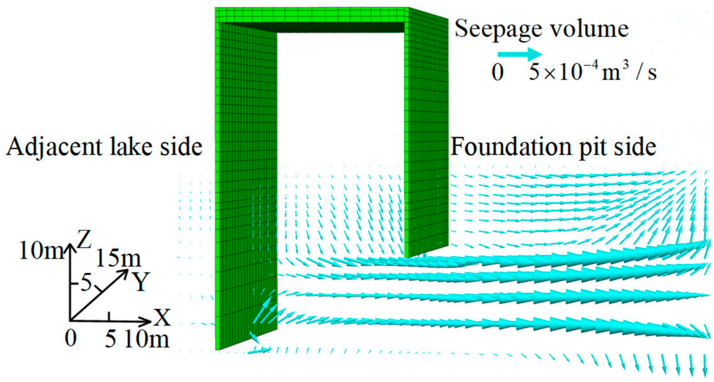

(**b**)

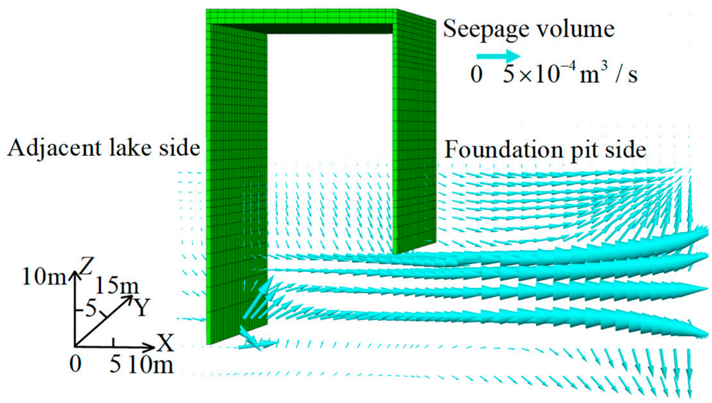

(**c**)

Figure 10. Vector distribution of seepage in lake into the weir under different working conditions. (**a**) Condition 2. (**b**) Condition 4. (**c**) Condition 6.

The water in the lake could bypass the steel sheet pile's seepage; in the process of foundation pit dewatering, the pore water pressure in the foundation pit decreased sharply, and pore water pressure difference was formed inside and outside the cofferdam. With the advancement in construction, the pore water pressure difference inside and outside the cofferdam gradually increased; the water in the lake bypassed the steel sheet pile seepage faster, while the horizontal displacement of the steel sheet pile gradually increased.

4.3. Mechanical Properties of Steel Sheet Pile Cofferdam after Construction Completion

(1) Vertical stress and settlement of steel cofferdam

The vertical stress simulation results of the steel cofferdam at different positions after the completion of the tunnel's construction are shown in Figure 11a. It can be seen that after construction was complete, the vertical stress at the top of the cofferdam showed compressive stress; from the lakeside to the foundation pit side, the vertical stress first increased with depth, increased to a maximum value of 0.23 MPa at 0.26 m, gradually decreased and tended to stabilize (all less than 0.01 MPa) at 0.26 m to 12.84 m, and gradually increased to the maximum value (0.23 MPa) at 12.84 m to 13.00 m (near the foundation pit of the cofferdam). On the lakeside, the vertical stress of the steel sheet pile showed compressive stress, which first increased with depth, increased to the maximum value (1.42 MPa) at 15.57 m, and gradually decreased at 15.57 m to 23.00 m (at the bottom of the steel sheet pile). On the foundation pit side, the vertical stress of the steel sheet pile showed compressive stress, which first increased with depth, increased to the maximum value (1.28 MPa) at 12.54 m, and then gradually decreased from 12.54 m to 13.00 m (at the bottom of the steel sheet pile). After the construction was complete, the maximum vertical stress of the steel cofferdam was 1.42 MPa, and the steel sheet pile cofferdam did not form a penetrating compression failure zone.

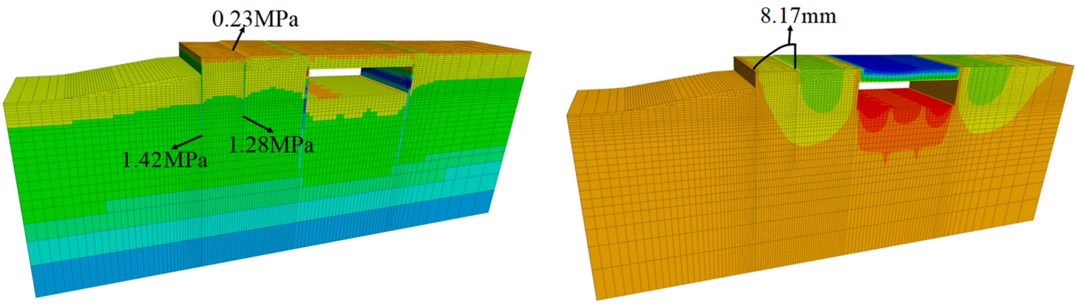

(**a**) (**b**)

Figure 11. Distribution of vertical stresses and settlements after the completion of tunnel construction. (**a**) Vertical stress. (**b**) Settlement.

The simulation results of the steel cofferdam's settlement after the completion of tunnel construction are shown in Figure 11b. It can be seen that from the side of the foundation pit to the side of the adjacent lake, the settlement of the cofferdam first increased and then decreased, reaching a maximum value of 8.17 mm at a distance of 0.53 m from the foundation pit; the settlement distribution was basically consistent with the distribution characteristics of vertical stress. The vertical stress and settlement in the steel sheet pile cofferdam caused by the tunnel's construction was relatively small, indicating that the bagged soil, geotextile and backfill soil laid on the water-facing side during construction could effectively suppress the settlement of the top of the cofferdam.

(2) Horizontal displacement of steel cofferdam

The simulation results of the horizontal displacement of the steel cofferdam after the completion of the steel tunnel construction are shown in Figure 12. It can be seen that after the construction was complete, there was an obvious settlement on the side cofferdam of the foundation pit; as the distance from the foundation pit increased, the settlement gradually decreased, and the overall horizontal displacement of the cofferdam was small, indicating that the steel sheet pile and round steel tie rod could ensure the overall stiffness of the cofferdam and limit its horizontal displacement. According to the simulation results of the deformation (settlement and horizontal displacement) of the steel sheet pile cofferdam, the steel cofferdam tilted to one side of the foundation pit as a whole, with a tilt angle of 3.37°, and the disturbance of the tunnel's construction to the cofferdam was relatively small.

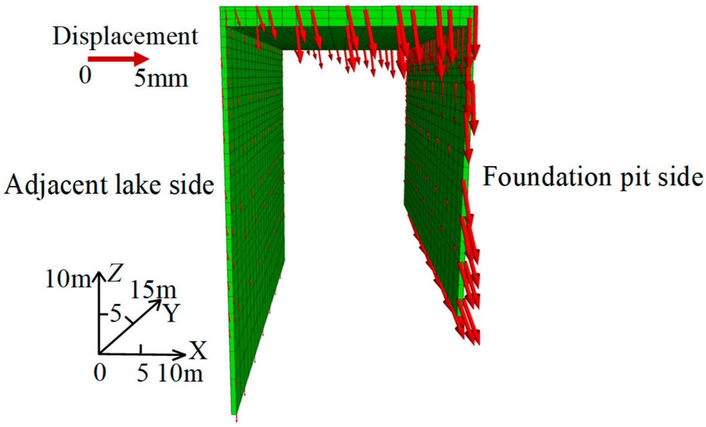

Figure 12. Distributions of horizontal displacements in cofferdam after the completion of tunnel construction.

(3) Axial force on tie rod in steel cofferdam

The tie rods in the steel cofferdam were numbered according to the positive direction of the Y-axis, and the axial force of the tie rods numbered 2, 4, 6, 8, 10, 12, and 14 was extracted. After the completion of the tunnel's construction, the simulation results of different tie rod axial forces in the steel cofferdam are shown in Figure 13.

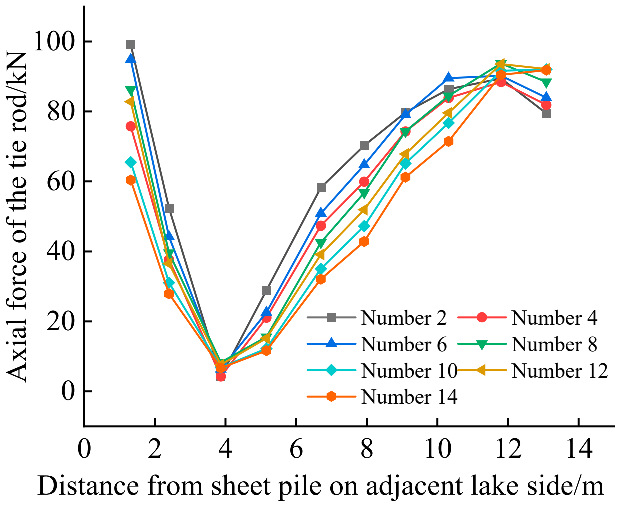

Figure 13. Axial forces of round steel ties at various locations in steel cofferdam.

It can be seen that the distribution of different tie rod axial forces was consistent: the maximum tension of 99.078 kN appeared on the side of the adjacent lake, and the maximum tension of 85.834 kN appeared on the side of the foundation pit; from the side of the adjacent lake to the side of the foundation pit, the axial force first decreased and then increased, while the overall distribution was a V-shape.

5. Conclusions

Based on the actual construction, using actual monitoring data and the numerical simulation results of the finite difference method, this study explored the mechanical properties of adjacent steel sheet pile cofferdams during the open-cut of lake water tunnels, and drew the following conclusions:

(1) During the construction, the maximum settlement of the steel sheet pile cofferdam under different construction conditions occurred at a distance from 0.27 to 0.53 m at the

side of the foundation pit. The maximum horizontal displacement of steel sheet piles appeared at a depth of 11.73 m on the adjacent lakeside, and at the bottom of the steel sheet piles on the foundation pit side. The tie rods in the steel cofferdam were distributed in a U-shape from the adjacent lake side to the foundation pit side and showed a pattern that first decreased and then increased, with the maximum value appearing on the foundation pit side.

(2) After the construction was complete, the settlement of the cofferdam increased first and then decreased from the side of the foundation pit to the side of the adjacent lakeside. The maximum value was reached at a distance of 0.53 m from the foundation pit. The cofferdam as a whole tilted toward the side of the foundation pit. The maximum tension of the tie rods' axial force on the side of the adjacent lakeside was 99.078 kN, and the maximum tension on the foundation pit side was 85.834 kN.

(3) In actual construction, the settlement and horizontal displacement of the steel cofferdam mainly occurred during tunnel construction; therefore, it was necessary to use temporary support to ensure the safety of steel sheet pile cofferdams during tunnel construction. In addition, the distribution characteristics of the axial force of the tie rods in the steel cofferdam should be comprehensively considered, and the number, spacing, and relative positions of the tie rods reasonably determined to optimize the design.

Author Contributions: Writing—review & editing, C.K.; Supervision, J.X. All authors have read and agreed to the published version of the manuscript.

Funding: This research was funded by the Natural Sciences Foundation Committee of China under Grant no. 41472254.

Institutional Review Board Statement: Not applicable.

Informed Consent Statement: Not applicable.

Data Availability Statement: The data used to support the findings of this study are included within the article.

Conflicts of Interest: The authors declare no conflict of interest regarding the publication of this paper.

References

1. Verstov, V.V.; Yudina, A.F.; Gaido, A.N. Improving Efficiency of Arranging Offshore Cofferdams. *Soil Mech. Found. Eng.* **2020**, *57*, 73–76. [CrossRef]
2. Byfileld, M.P.; Crawford, R.J. Oblique bending in U-shape steel pile. *Struct. Build.* **2003**, *156*, 255–261. [CrossRef]
3. Bourne, P.J.; Potts, D.M.; Rowbottm, D. Plastic bending of steel sheet piles. *Geotech. Eng.* **2007**, *160*, 129–140. [CrossRef]
4. Osthoff, D.; Jurgen, G. Deformation behavior of steel sheet pile during jacking. *Comput. Geotech.* **2018**, *101*, 1–10. [CrossRef]
5. Lefas, I.D.; Georgiannou, V.N. Analysis of a cofferdam support and design implications. *Comput. Struct.* **2001**, *79*, 2461–2469. [CrossRef]
6. Gui, M.W.; Han, K.K. An investigation on a failed double-wall cofferdam during construction. *Eng. Fail. Anal.* **2009**, *16*, 421–432. [CrossRef]
7. Shao, J.H.; Fan, Z.F.; Huang, Y.Y.; Zhan, Y.L.; Cai, Q.H. Multi-objective optimization of double-walled steel cofferdams based on response surface methodology and particle swarm optimization algorithm. *Structures* **2023**, *49*, 256–266. [CrossRef]
8. Yan, Z.; Zhang, H.Q.; Xiao, Z.; Yuan, Y.; Shen, Z.C. Centrifuge tests on lateral bearing behaviors of double steel sheet pile structures on marine soft grounds. *Appl. Ocean Res.* **2023**, *134*, 103538. [CrossRef]
9. Li, P.; Sun, X.F.; Chen, J.J.; Shi, J.W. Effects of new construction technology on performance of ultralong steel sheet pile cofferdams under tidal action. *Geomech. Eng.* **2021**, *27*, 561–571.
10. Cao, H.; Luo, Y.; Zhou, H.X. Analysis of permeability of cofferdam with armor-plate pile for xingguang bridge's pier. *Chin. J. Rock Mech. Eng.* **2006**, *25*, 152–157.
11. Fukumoto, Y.; Yang, H.X.; Hosoyamada, T.; Ohtsuka, S. 2-D coupled fluid-particle numerical analysis of seepage failure of saturated granular soils around an embedded sheet pile with no macroscopic assumptions. *Comput. Geotech.* **2021**, *136*, 104234. [CrossRef]
12. Abbasi, H.; Binesh, S.M.; El Naggar, M.H. Response analysis of single pile embedded in saturated sand under bidirectional cyclic loading. *Soil Dyn. Earthq. Eng.* **2023**, *166*, 107756. [CrossRef]
13. Xu, F.; Li, S.C.; Zhang, Q.Q.; Li, L.P.; Zhang, Q.; Wang, K.; Liu, H.L. Analysis and design implications on stability of cofferdam subjected to water wave action. *Mar. Georesour. Geotechnol.* **2016**, *34*, 181–187. [CrossRef]

14. Gao, L.; Xu, Z.; Wang, Q.; Zhang, Z.; Li, P. Model test study on deformation of snowflake shaped steel sheet pile based on OFDR. *Sensors* **2021**, *21*, 7062. [CrossRef]
15. Kim, G.; Ham, K.; Lee, J. Effects of Surface Roughness on Lateral Load–Carrying Capacities of Piles Embedded in Sand. *J. Geotech. Geoenviron. Eng.* **2020**, *146*, 04020064. [CrossRef]
16. Doubrovsky, M.P.; Meshcheryakov, G.N. Physical modeling of sheet piles behavior to improve their numerical modeling and design. *Soils Found.* **2015**, *55*, 691–702. [CrossRef]
17. Schreter, M.; Neuner, M.; Unteregger, D.; Hofstetter, G. On the importance of advanced constitutive models in finite element simulations of deep tunnel advance. *Tunn. Undergr. Space Technol.* **2018**, *80*, 103–113. [CrossRef]
18. Liao, P.; Ni, P.; Ma, B.; Sun, W.; Wang, A. Centrifuge and numerical modeling of brittle damage of buried pipelines subjected to tunneling induced ground settlements. *Tunn. Undergr. Space Technol.* **2023**, *138*, 105158. [CrossRef]
19. Pascariello, M.N.; Luciano, A.; Bilotta, E.; Acikgoz, S.; Mair, R. Numerical modelling of the response of two heritage masonry buildings to nearby tunnelling. *Tunn. Undergr. Space Technol.* **2023**, *131*, 104845. [CrossRef]
20. Bahri, M.; Mascort-Albea, E.J.; Romero-Hernández, R.; Koopialipoor, M.; Soriano-Cuesta, C.; Jaramillo-Morilla, A. Numerical Model Validation for Detection of Surface Displacements over Twin Tunnels from Metro Line 1 in the Historical Area of Seville (Spain). *Symmetry* **2022**, *14*, 1263. [CrossRef]
21. Jin, H.; Yuan, D.; Zhou, S.; Zhao, D. Short-Term and Long-Term Displacement of Surface and Shield Tunnel in Soft Soil: Field Observations and Numerical Modeling. *Appl. Sci.* **2022**, *12*, 3564. [CrossRef]
22. Li, L.; Fan, H.; Liu, H.; Li, S.; Cheng, S.; Zhang, Q.; Tu, W.; Zhou, S. Model test and numerical simulation research on the mechanical response law of lager span and small interval tunnels constructed by CD method. *Tunn. Undergr. Space Technol.* **2023**, *132*, 104947. [CrossRef]
23. Abate, G.; Massimino, M.R. Numerical modelling of the seismic response of a tunnel–soil–aboveground building system in Catania (Italy). *Bull. Earthq. Eng.* **2017**, *15*, 469–491. [CrossRef]
24. Wu, Y.B.; Ye, J.B.; Ge, H.B.; Liu, G.Q.; Liu, H.W. Numerical investigation of dual-row batter pile wall in deep excavation. *Mech. Adv. Mater. Struct.* **2021**, *29*, 5793–5807. [CrossRef]
25. Wu, J.; Zhou, Z.F.; Xia, W.J.; Wang, H.X.; Fang, Z.Q. A Novel Excavation and Construction Method for an Extra-Long Underwater Tunnel in Soft Soils. *Adv. Civ. Eng.* **2021**, *2021*, 6184411. [CrossRef]
26. Lin, Y.F.; Cheng, W.Z.; Zhu, H.H. Researches on interaction between exceeding deep footing groove in rivers and cofferdam. *Chin. J. Geotech. Eng.* **2006**, *28* (Suppl. S1), 1826–1829.
27. Fall, M.; Guo, Z.G.; Ndiaye, B.C. Three-dimensional response of double anchored sheet pile walls subjected to excavation and construction sequence. *Heliyon* **2019**, *5*, e01348. [CrossRef] [PubMed]
28. Wang, J.J.; Jiang, Z.J.; Li, F.; Chen, W.M. The prediction of water level based on support vector machine under construction condition of steel sheet pile cofferdam. *Concurr. Comput. Pract. Exp.* **2021**, *33*, e6003. [CrossRef]
29. Zhao, W.; Du, C.; Sun, L.; Chen, X. Field measurements and numerical studies of the behaviour of anchored sheet pile walls constructed with excavating and backfilling procedures. *Eng. Geol.* **2019**, *259*, 105165. [CrossRef]
30. Gu, X.Q.; Wu, R.T.; Liang, F.Y.; Gao, G.Y. On HSS model parameters for Shanghai soils with engineering verification. *Rock Soil Mech.* **2021**, *42*, 833–845.